

Theoretical polarization dependence of the two-phonon double-resonant Raman spectra of graphene

Valentin N. Popov

Faculty of Physics, University of Sofia, BG-1164 Sofia, Bulgaria

Philippe Lambin

*Research Center in Physics of Matter and Radiation,
Facultés Universitaires Notre Dame de la Paix, B-5000 Namur, Belgium*

(Dated: November 16, 2018)

Abstract

The experimental Raman spectra of graphene exhibit a few intense two-phonon bands, which are enhanced through double-resonant scattering processes. Though there are many theoretical papers on this topic, none of them predicts the spectra within a single model. Here, we present results for the two-phonon Raman spectra of graphene calculated by means of the quantum perturbation theory. The electron and phonon dispersions, electronic lifetime, electron-photon and electron-phonon matrix elements, are all obtained within a density-functional-theory-based non-orthogonal tight-binding model. We study systematically the overtone and combination two-phonon Raman bands, and, in particular, the energy and polarization dependence of their Raman shift and intensity. We find that the ratio of the integrated intensities for parallel and cross polarized light for all two-phonon bands is between 0.33 and 0.42. Our results are in good agreement with the available experimental data.

I. INTRODUCTION

Presently, graphene is considered as a prospective material for nanoelectronics and nanophotonics.^{1,2} Among the various experimental techniques, the Raman spectroscopy has proven to be an indispensable tool for investigation of this material.³⁻⁶

Graphene has a single Raman-active phonon E_{2g} observed as an intense line (the G band) in the first-order Raman spectra. The second-order spectra of graphene with low defect density has several intense bands, which originate from scattering of electrons and holes by two phonons of the same/different frequency and non-zero momentum and are called overtone/combination bands. The appearance of intense second-order bands can be explained by the double-resonant (DR) scattering mechanism.^{7,8} These bands contain valuable information on the phonon dispersion⁹⁻¹² and the electron-phonon and electron-electron matrix elements.¹³ The Raman spectra of graphene with defects show additional bands, which arise from DR scattering of electrons and holes by phonons and defects.

The theoretical investigation of the two-phonon DR scattering in graphene has been performed using various approximations: replacement of the electron-photon and electron-phonon interactions with constants, using a constant electronic lifetime, considering only high-symmetry directions in the Brillouin zone, as well as exact DR conditions. The predicted dispersive behavior of the Raman bands⁷ and the frequency shift of the Stokes and anti-Stokes Raman bands¹⁴ have been found in quantitative agreement with the experimental data. It has also been realized that the integration⁹ over the entire Brillouin zone of graphene is essential for predicting the Raman intensity.^{15,16} While most of the theoretical papers focus on the most intense overtone band, in a recent study, all two-phonon Raman bands with observable intensity have been calculated using an electron-phonon matrix element derived within a nearest-neighbor π -band tight-binding model.¹⁷ The dominant contribution to the two-phonon bands from different parts of the Brillouin zone^{17,18} and from different scattering processes¹⁷ has also been discussed. The polarization dependence of the most intense overtone band has been studied experimentally and theoretically.¹⁹ The progress, made so far in the modeling of the DR bands, has been achieved either with simple π -band tight-binding models, or with more sophisticated models but relying on approximations of the electron-phonon matrix element, and in most cases concerns only a few intense bands. Our experience indicates that, although the Raman shift of the bands is not sensitive to the

used matrix element, their Raman intensity crucially depends on it.

Here, we calculate the two-phonon DR Raman spectra of graphene using a non-orthogonal tight-binding (NTB) model, which implements parameters derived from a density functional theory (DFT) study and thus has no adjustable parameters.²⁰ In particular, the electronic²¹ and phonon²² dispersion, the electron-photon and electron-phonon matrix elements,²³ as well as the electronic linewidth²⁴ are all obtained within this model. The NTB model for electrons and phonons in graphene is introduced in Sec. II. The calculated two-phonon DR Raman spectra of graphene and its polarization dependence are discussed in Sec. III. The paper ends up with conclusions (Sec. IV).

II. THEORETICAL PART

A. The NTB model

We use a NTB model with four valence electrons per carbon atom to calculate the electronic dispersion of graphene.²¹ This model is based on matrix elements of the Hamiltonian and overlap matrix elements derived from DFT²⁰ and therefore it does not rely on any adjustable parameters. It also allows one to estimate the total energy and the forces on the atoms. This feature is utilized for relaxation of the atomic structure. Up to a few electron volts away from the Fermi energy, the electronic structure of graphene has the form of conic valence and conduction bands (Dirac cones) with a common apex (the Dirac point) at two non-equivalent special points, K and K', of the Brillouin zone. This specific form of the electronic bands plays an important role in the enhancement of the two-phonon Raman scattering through the DR mechanism.

The dynamical model of graphene uses a dynamical matrix derived by a perturbative approach within the NTB model.²² The electron-photon and electron-phonon matrix elements are calculated explicitly.²³ The summation over the Brillouin zone in the first-order perturbation term of the dynamical matrix is performed over a 40×40 mesh of \mathbf{k} points, for which the phonon frequencies converge within 1 cm^{-1} . The calculated in-plane phonon branches of graphene, after scaling by a factor of 0.9, agree fairly well with the available experimental data²² (Fig. 1). The phonons with displacement in the graphene plane (in-plane phonons) can interact with electrons and thus can contribute to the Raman spectra.

Those with atomic displacement perpendicular to graphene (out-of-plane phonons) are less well reproduced but they do not contribute to the spectra.

It will be shown below that only phonons, close to the high-symmetry directions ΓK , ΓM , and KM of the Brillouin zone, are of major importance for the two-phonon spectra. The phonon branches along these directions will be denoted, as usual, by two-letter acronyms describing their vibrational pattern: the letters O and A stand for “optical” and “acoustic”, respectively; the letters L, T, and Z denote in-plane longitudinal, in-plane transverse, and out-of-plane atomic displacement, respectively. The acronyms for the branches along the KM direction will be primed. Alternatively, for each wavevector, the phonons will be ascribed the index ν , $\nu = 1, \dots, 6$, in order of increasing frequency. The phonons with a certain ν can belong to branches with a different vibrational pattern. For example, a phonon with $\nu = 6$ can belong to the LO or TO branch. It will also be argued that only phonons close to the Γ and K points give a significant contribution to the two-phonon Raman spectra. Such phonons will be denoted by acronyms ending with @ Γ and @K. For example, LO phonons close to the Γ point will be denoted by LO@ Γ and TO phonons close to the K point along the KM direction will be denoted by TO’@K (see, Fig. 1).

B. The double-resonant processes

The amplitude for two-phonon DR Raman scattering processes in graphene is described by fourth-order terms in perturbation theory.²⁵ The underlying processes include virtual scattering of electrons/holes by phonons between states of the Dirac cone at the K point or the K’ point, or between states of the Dirac cones at the K and K’ points. The momentum is conserved in each virtual process but the energy is conserved only for the entire DR process. Below, we will consider only Stokes processes. In this case, a two-phonon DR process includes an absorption of a photon with a creation of an electron-hole pair, two consecutive processes of scattering of an electron/hole with creation of a phonon, and a recombination of the electron-hole pair with an emission of a photon (Fig. 2). There are altogether eight such processes.^{17,26} The total two-phonon Raman intensity is given by the expression

$$I \propto \sum_f \left| \sum_{c,b,a} \frac{M_{fc} M_{cb} M_{ba} M_{ai}}{(E_i - E_c - i\gamma)(E_i - E_b - i\gamma)(E_i - E_a - i\gamma)} \right|^2 \delta(E_i - E_f) \quad (1)$$

Here, the inner sum is the scattering amplitude. E_u , $u = i, a, b, c, f$, are the energies of the initial (i), intermediate (a, b, c), and final (f) states of the system of photons, electrons, holes, and phonons. In the initial state, only an incident photon is present and, therefore, $E_i = E_L$, where E_L is the incident photon energy. In the final state, there is a scattered photon and two created phonons. M_{uv} are the matrix elements for virtual processes between initial, intermediate, and final states. In particular, M_{ai} and M_{fc} are the matrix elements of momentum for the processes of creation and recombination of an electron-hole pair, respectively. M_{ba} and M_{cb} are the electron/hole-phonon matrix elements. γ is the sum of the halfwidths of pairs of electronic and hole states, and will be referred to as the electronic linewidth. The electron-photon and electron-phonon matrix elements, and the electronic linewidth are calculated explicitly.^{23,24} The Dirac delta function ensures energy conservation for the entire process. In the calculations, it is replaced by a Lorentzian with a halfwidth of 5 cm^{-1} . The summation over the intermediate states runs over all valence and conduction bands, and over all electron wavevectors \mathbf{k} . The summation over the final states runs over all phonon branches and phonon wavevectors \mathbf{q} . For both summations, convergence is reached with a 800×800 mesh of \mathbf{k} and \mathbf{q} points in the Brillouin zone.

For the discussion of the polarization dependence of the Raman intensity of the two-phonon bands, it is advantageous to rewrite Eq. (1) in the form

$$I \propto \sum_f |\mathbf{e}_S \cdot R \cdot \mathbf{e}_L|^2 \delta(E_i - E_f) \quad (2)$$

Here, \mathbf{e}_L and \mathbf{e}_S are the polarization vectors of the incident and scattered laser light, respectively, and R is the Raman tensor. Everywhere below we consider only backscattering geometry in accord with the usual experimental Raman setup for graphene and, therefore, the polarization vectors lie in the graphene plane.

III. RESULTS AND DISCUSSION

A. Electronic linewidth

The electronic linewidth γ is due to a large extent to scattering of the electrons (holes) by phonons and other electrons (holes). The majority of the published reports assume that γ is energy-independent. Recently, it has been argued that in undoped graphene γ is dominated by electron-phonon processes and the expression $\gamma = 9.44E + 3.40E^2$ has been derived, where the energy separation between the valence and conduction bands E is in eV and γ is in meV.¹⁷ Here, the electronic linewidth was calculated by summing up the contributions of all electron/hole-phonon scattering processes for all phonons in the Brillouin zone as a function of E . The obtained energy dependence was approximated in the range [1.0, 3.5] eV with the expression

$$\gamma = 12.60E + 3.45E^2 \quad (3)$$

For energies in this energy range, γ changes more than four times from 16 to 86 meV (Fig. 3).

B. Overtone bands

The calculated overtone Raman spectrum for $E_L = 2.0$ eV and parallel light polarization along a zigzag line of carbon bonds is shown in Fig. 4 (bottom). It has two intense bands ($2D$ and $2D'$) and three weaker ones ($2D^3$, $2D^4$, and $2D''$) and a much weaker one ($2D^5$). There are also other bands of in-plane phonons close to the Γ and K points but they are either very weak, or are in the shoulders of intense bands, and in both cases are practically unobservable.

The assignment of the overtone spectrum can be performed by analyzing the contribution of phonons with different ν and from different parts of the Brillouin zone of graphene. First, the contributions of the phonons with $\nu = 2, \dots, 6$ are given in Fig. 4 (top five graphs). The bands in these spectra originate from pairs of phonons TA@ Γ ($\nu = 2$), LA@ Γ and TA@K ($\nu = 3$), LA@K ($\nu = 4$), TO@K ($\nu = 5$), and TO'@K and LO@K ($\nu = 6$) (see also Fig. 1). The contributions for $\nu = 5, 6$ are by about three orders of magnitude larger than the remaining ones.

Secondly, the assignment of the Raman bands to definite phonons at the Γ and K points is supported by the analysis of the contributions to the spectra from different parts of the Brillouin zone for parallel light polarization with averaging over all orientations in the graphene plane. In Fig. 5, the regions with major contribution to the bands are given by shaded areas. In particular, the $2D^3$ band comes from phonons TA@ Γ along the ΓK direction, the $2D^4$ band - from phonons LA@ Γ along ΓM , the $2D''$ band - from phonons LA@K along ΓK (not shown in Fig. 5), and the $2D'$ band - from phonons LO@ Γ from all directions in the Brillouin zone. The $2D$ band originates from phonons TO@K and TO'@K, which contribute to the integrated Raman intensity of this band in ratio $\approx 10 : 1$. It has long been accepted that the dominant contribution to the $2D$ band comes from phonons along the KM direction and that the contribution along the ΓK direction vanishes because of interference.¹⁶ Our graphs in Fig. 4 and 5 for $\nu = 5, 6$ confirm the recent conclusion that the main contribution to this band comes from the ΓK direction and only a small part comes from the KM direction.^{17,18} We also confirm the result of Ref.¹⁷, that among the eight DR processes, those with scattering of an electron and a hole have dominant contribution to the bands.

The overtone bands are dispersive, i.e., their Raman shift depends on the laser energy (Fig. 6). The shift increases (decreases) due to increase (decrease) of the phonon frequency away from the Γ and K points. It is approximately linear in E_L with slopes of ≈ 0 for the $2D'$ band, $89 \text{ cm}^{-1}/\text{eV}$ ($2D$ band), $-193 \text{ cm}^{-1}/\text{eV}$ ($2D''$), $419 \text{ cm}^{-1}/\text{eV}$ ($2D^4$), and $256 \text{ cm}^{-1}/\text{eV}$ ($2D^3$) at $E_L = 2.0 \text{ eV}$. The slope of the $2D$ band corresponds to the experimental one of $88 \text{ cm}^{-1}/\text{eV}$ (Ref. [11]).

The integrated Raman intensity of the overtone bands (Fig. 7) is quasi-linear in E_L except for the $2D^3$ band. The ratio of the integrated intensities $A(2D)/A(2D')$ has been discussed a lot in the literature because it is related to the electron-phonon matrix elements at the K and Γ points. Here, we find that this ratio depends on the energy: it varies from 4.7 for $E_L = 1.0 \text{ eV}$ to 15.0 for $E_L = 3.5 \text{ eV}$; for $E_L = 2.4 \text{ eV}$ it is equal to 8.7. By contrast, recent sophisticated DFT-GW calculations¹⁷ yield 21.5, which is several times larger than our value. The reason for this disagreement can be found in the use of GW corrected electron-phonon matrix elements for the LO phonon at the Γ point and the TO phonon at the K point. While the ratio of the squares of these matrix elements at the two points derived by DFT is $M_K^2/M_\Gamma^2 = 2.02$, the DFT-GW result is 3.03 (Ref. [27]). Since the Raman

intensity depends on the square of this ratio, the DFT-GW gives an intensity ratio that is larger than the DFT one by a factor of 2.25. Our result, corrected by the same correction factor, is 19.6. Both theoretical results underestimate the experimental values of 26 (Ref. [28]) and 27 (Ref. [3]) by $\sim 25\%$. The origin of this underestimation is still unknown.

C. Combination bands

The combination Raman spectrum is calculated for $E_L = 2.0$ eV and parallel light polarization along a zigzag line of carbon bonds (Fig. 8, bottom). The spectrum is dominated by two intense bands: $D + D''$ and a higher frequency one, which originate from the branches $5 + 4$ and $6 + 5$, respectively. There are also four other less intense bands: $D' + D^3$, $D' + D^4$, and $D + D^5$.

As above, the assignment is facilitated by considering the contributions to these bands from pairs of phonons with $\nu, \nu' = 2, 3, 4, 5, 6$. It is seen in Fig. 8 (top six graphs) that for each pair $\nu + \nu'$ there is a single band. These bands are due to pairs of phonons TOTA@K ($\nu + \nu' = 5 + 3$), TOLA@K ($5 + 4$), LOTA@ Γ ($6 + 2$), LOLA@ Γ ($6 + 3$), TO'LO'@K ($6 + 4$), and TO'LA'@K ($6 + 5$) (see also Fig. 1). Unlike the case of the overtone bands, the intensity of the various combination bands varies only by one order of magnitude. The band $D + D''$ is mainly due to phonons TOLA@K with a small contribution of phonons TO'LO'@K. The phonons TO'LA'@K give rise to an intense band at ~ 2700 cm^{-1} . The large contribution of the phonons TO'LO'@K and TO'LA'@K is consistent with the large electron-phonon matrix element for the phonon TO'@K and the nonzero matrix element for the phonons LA'@K and LO'@K. We note that the latter contribute to the overtone spectra as well but their bands are masked in the shoulder of the intense $2D$ band. The band at 2700 cm^{-1} also overlaps considerably with the much more intense $2D$ band and cannot be observed as a separate feature. Thus, the total Raman spectrum exhibits the intense $2D$ band, the two weak bands $2D'$ and $D + D''$ (Fig. 9), as well as the two very weak bands $D' + D^3$ and $D' + D^4$.

Similarly to the overtone bands, the combination bands are dispersive. The dependence of the Raman shift on the laser energy (Fig. 10) is almost linear with a slope of 74 cm^{-1}/eV for the highest-frequency band, -50 cm^{-1}/eV ($D + D''$), -54 cm^{-1}/eV ($D + D^5$), 210 cm^{-1}/eV ($D' + D^4$), and 123 cm^{-1}/eV ($D' + D^3$) at $E_L = 2.0$ eV. Each slope is equal approximately to the sum of half of the slopes of the corresponding overtone bands. The calculated energy

dependence of the $D + D''$ band frequency reproduces fairly well the experimental data but the derived slope is almost three times larger than the experimental one of $-18 \text{ cm}^{-1}/\text{eV}$ for energies between 1.92 and 2.71 eV (Ref. [11]). The calculated frequencies for the $D' + D^4$ and $D' + D^3$ bands underestimate the Raman data up to 80 and 30 cm^{-1} , respectively. Similar underestimation is present in other precise calculations.^{17,29} On the other hand, the frequency slopes of the bands $D' + D^4$ and $D' + D^3$ are in fair agreement with the measured ones of $221 \text{ cm}^{-1}/\text{eV}$ and $140 \text{ cm}^{-1}/\text{eV}$, respectively.³⁰ We note that neither we, nor the authors of Ref. [17], have found any observable combination band for phonons TOLA@ Γ though such band has been established³⁰ by fitting a low-intensity Raman band with two Lorentzians for two overlapping bands assigned to phonons TOLA@ Γ and LOLA@ Γ .

The calculated integrated Raman intensity is shown in Fig. 11. The curves are increasing functions of laser energy for all bands except for the band $D' + D^3$ and the highest frequency one. For the most studied $D + D''$ band, we find $A(2D)/A(D + D'') = 12.2$. Introducing the DFT-GW correction factor for the electron-phonon matrix element of the TO phonon at the K point of 1.76 (Ref.²⁷), for the latter ratio we obtain the value of 21.5, which agrees with the previous estimate¹⁷ of 16 and the experimental one³ of ≈ 21 . The inset of Fig. 11 shows the dependence of the DFT-GW corrected ratios $A(2D')/A(2D)$ and $A(D + D'')/A(2D)$ as a function of E_L . Both curves agree well with the theoretical ones¹⁷ and the available experimental data.³

D. Dependence on the electronic linewidth

Most of the previously reported two-phonon Raman spectra have been calculated for energy-independent γ . In order to study the effect of this approximation we performed calculation of the integrated intensity A_c for constant linewidth $\gamma_c = \gamma(E_L = 2.0 \text{ eV}) = 39 \text{ meV}$ as well. We found that, for any of the two-phonon peaks discussed above, the calculated ratio of the integrated intensities, A and A_c , for variable and constant linewidth, respectively, can be fitted very well with the expression $A/A_c = (\gamma_c/\gamma)^2$. Therefore, A can be written as $A = f/\gamma^2$, where f depends on E_L and does not depend on γ . It is clear from Figs. 7 and 11 that the rate of change of f as a function of E_L is different for the different two-phonon bands. Thus, the ratio of the integrated intensities for any pair of two-phonon bands 1 and 2, $A_1/A_2 = f_1/f_2$, should depend on E_L in agreement with the recent conclusions.¹⁷ We

note that, in the latter paper, deviation from the $1/\gamma^2$ behavior has been found. The correct dependence should be established by comparison with experimental Raman data collected at more values of the laser energy.

The intensity ratio for the $2D$ and $2D'$ overtone bands can be obtained using the simple tight-binding analytical formulas:³¹ $A(2D) \propto 2(\gamma_K/\gamma)^2$ and $A(2D') \propto (\gamma_\Gamma/\gamma)^2$. Here, $\gamma = \gamma_\Gamma + \gamma_K$ is the total electronic linewidth; $\gamma_{\Gamma,K} \propto E_L M_{\Gamma,K}^2 / \omega_{\Gamma,K}$ are the linewidths due to the LO phonon at the Γ point and the TO phonon at the K point, $M_{\Gamma,K}^2$, and $\omega_{\Gamma,K}$ are the corresponding square of the electron-phonon matrix element and the phonon frequency, respectively. The predicted ratio of the integrated intensity of the two bands is a constant, equal to 3 (or 7.9), evaluated with electronic linewidth from DFT (or DFT-GW).²⁷ The latter values are about 7 (or 2.7) times smaller than those of the precise derivations at $E_L = 2.4$ eV, presented here and in Ref. [17]. The disagreement for the intensity ratio can be sought in the approximations used in the theoretical scheme of Ref. [31].

E. Polarization dependence of the bands

Let us choose a coordinate system in the graphene plane with x axis along a zigzag line of carbon bonds (and therefore the y axis is along an armchair line of carbon bonds), and set $\mathbf{e}_L = (\cos \alpha, \sin \alpha)$ and $\mathbf{e}_S = (\cos \beta, \sin \beta)$. In the case of parallel and cross polarizations, the intensity is not angle-dependent because of the high-symmetry of graphene. On the contrary, for fixed polarization angle and variable analyzer angle, or vice versa, the intensity depends only on the difference $\alpha - \beta$ and does not depend on the sign of this difference. Therefore, the Raman intensity, Eq. (2), can be written as

$$I = (I_{\parallel} - I_{\perp}) \cos^2(\alpha - \beta) + I_{\perp} \quad (4)$$

The intensity for parallel and cross polarized light, I_{\parallel} and I_{\perp} , can be obtained by fitting this expression to the calculated angular dependence of the intensity. Expression, similar to Eq. (4), holds for the integrated intensity as well.

Fig. 12 shows the polarization dependence of the ratio of the calculated integrated intensities A_{\perp}/A_{\parallel} at $E_L = 2.0$ eV. As could be expected, all two-phonon bands have similar angular dependence of the Raman intensity, which follows from Eq. (4). The derived values of the ratio A_{\perp}/A_{\parallel} are: 0.3678 ($2D^3$), 0.4195 ($2D^4$), 0.3321 ($2D''$), 0.3377 ($2D$), 0.4075

($2D'$), $0.3718 (D' + D^3)$, $0.4073 (D' + D^4)$, $0.3401 (D + D^5)$, $0.3350 (D + D'')$. The intensity ratio for all bands is between 0.33 and 0.42. The ratio for the $2D$ band corresponds to the value $1/3$ derived within a simple tight-binding model³¹ and the tight-binding estimate¹⁹ of 0.32, and is in fair agreement with the experimental value¹⁹ of 0.3. So far as we are aware, there are no reports on the polarization dependence of the other two-phonon bands.

IV. CONCLUSIONS

We have presented a complete theoretical treatment of the two-phonon Raman bands of graphene within a non-orthogonal tight-binding model with no adjustable parameters and no other approximations. We have calculated the laser energy and polarization dependence of the Raman shift and intensity. In particular, the ratio of the integrated Raman intensity for parallel and cross polarized light for all bands is between 0.33 and 0.42. The agreement of our results with available experimental data is very good and the predictions can be used for further comparison to experiment and for support in the assignment of the two-phonon Raman spectra. Furthermore, we have made definite conclusions on the dominant contributions to the Raman scattering amplitude. Our computations can easily be extended to include higher-order Raman processes.

ACKNOWLEDGMENTS

V.N.P. acknowledges financial support from Facultés Universitaires Notre Dame de la Paix, Namur, Belgium, and Grant No.71/05.04.2012 of University of Sofia, Sofia, Bulgaria.

¹ A. K. Geim and K. S. Novoselov, *Nature Materials* **6**, 183 (2007).

² F. Bonaccorso, Z. Sun, T. Hasan, and A. C. Ferrari, *Nature Photonics* **4**, 611 (2010).

³ A. C. Ferrari, J. C. Meyer, V. Scardaci, C. Casiraghi, M. Lazzeri, F. Mauri, S. Piscanec, D. Jiang, K. S. Novoselov, S. Roth, and A. K. Geim, *Phys. Rev. Lett.* **97**, 187401 (2006).

⁴ L. M. Malard, M. A. Pimenta, G. Dresselhaus, and M. S. Dresselhaus, *Phys. Rep.* **473**, 51 (2009).

- ⁵ M. S. Dresselhaus, A. Jorio, M. Hofmann, G. Dresselhaus, and R. Saito, *Nano Lett.* **10**, 751 (2010).
- ⁶ V. Zólyomi, J. Koltai, and J. Kúrti, *Phys. Stat. Sol. B* **248**, 2435 (2011).
- ⁷ C. Thomsen and S. Reich, *Phys. Rev. Lett.* **85**, 5214 (2000).
- ⁸ S. Reich and C. Thomsen, *Phil. Trans. R. Soc. Lond. A* **362**, 2271 (2004).
- ⁹ R. Saito, A. Jorio, A. G. SouzaFilho, G. Dresselhaus, M. S. Dresselhaus, and M. A. Pimenta, *Phys. Rev. Lett.* **88**, 027401 (2002).
- ¹⁰ A. Grüneis, R. Saito, T. Kimura, L. G. Cançado, M. A. Pimenta, A. Jorio, A. G. SouzaFilho, G. Dresselhaus, and M. S. Dresselhaus, *Phys. Rev. B* **65**, 155405 (2002).
- ¹¹ D. L. Mafra, G. Samsonidze, L. M. Malard, D. C. Elias, J. C. Brant, F. Plentz, E. S. Alves, and M. A. Pimenta, *Phys. Rev. B* **76**, 233407 (2007).
- ¹² A. Grüneis, J. Serrano, A. Bosak, M. Lazzeri, S. L. Molodtsov, L. Wirtz, C. Attaccalite, M. Krisch, A. Rubio, F. Mauri, and T. Pichler, *Phys. Rev. B* **80**, 085423 (2009).
- ¹³ D. M. Basko, S. Piscanec, and A. C. Ferrari, *Phys. Rev. B* **80**, 165413 (2009).
- ¹⁴ L. G. Cançado, M. A. Pimenta, R. Saito, A. Jorio, L. O. Ladeira, A. Grueneis, A. G. SouzaFilho, G. Dresselhaus, and M. S. Dresselhaus, *Phys. Rev. B* **66**, 035415 (2002).
- ¹⁵ J. Maultzsch, S. Reich, and C. Thomsen, *Phys. Rev. B* **70**, 155403 (2004).
- ¹⁶ R. Narula and S. Reich, *Phys. Rev. B* **78**, 165422 (2008).
- ¹⁷ P. Venezuela, M. Lazzeri, and F. Mauri, *Phys. Rev. B* **84**, 035433 (2011).
- ¹⁸ R. Narula, N. Bonini, N. Marzani, and S. Reich, *Phys. Stat. Sol. B* **248**, 2635 (2011).
- ¹⁹ D. Yoon, H. Moon, Y.-W. Son, G. Samsonidze, B. H. Park, J. B. Kim, Y. P. Lee, and H. Cheong, *Nano Lett.* **8**, 4270 (2008).
- ²⁰ D. Porezag, T. Frauenheim, T. Köhler, G. Seifert, and R. Kaschner, *Phys. Rev. B* **51**, 12 947 (1995).
- ²¹ V. N. Popov and L. Henrard, *Phys. Rev. B* **70**, 115407 (2004).
- ²² V. N. Popov and P. Lambin, *Phys. Rev. B* **73**, 085407 (2006).
- ²³ V. N. Popov, L. Henrard, and P. Lambin, *Phys. Rev. B* **72**, 035436 (2005).
- ²⁴ V. N. Popov and P. Lambin, *Phys. Rev. B* **74**, 075415 (2006).
- ²⁵ R. M. Martin and L. M. Falicov, in *Light Scattering in Solids I*, Vol. 8, edited by M. Cardona (Springer-Verlag, Berlin, 1983).
- ²⁶ J. Kúrti, V. Zólyomi, A. Grüneis, and H. Kuzmany, *Phys. Rev. B* **65**, 165433 (2002).

- ²⁷ M. Lazzeri, C. Attaccalite, L. Wirtz, and F. Mauri, Phys. Rev. B **78**, 081406(R) (2008).
- ²⁸ F. Alzina, H. Tao, J. Moser, Y. García, A. Bachtold, and C. M. Sotomayor-Torres, Phys. Rev. B **82**, 075422 (2010).
- ²⁹ K. Sato, J. S. Park, R. Saito, C. Cong, T. Yu, C. H. Lui, T. F. Heinz, G. Dresselhaus, and M. S. Dresselhaus, Phys. Rev. B **84**, 035419 (2011).
- ³⁰ C. Cong, T. Yu, R. Saito, G. F. Dresselhaus, and M. S. Dresselhaus, ACS Nano **5**, 1600 (2011).
- ³¹ D. M. Basko, Phys. Rev. B **78**, 125418 (2008).

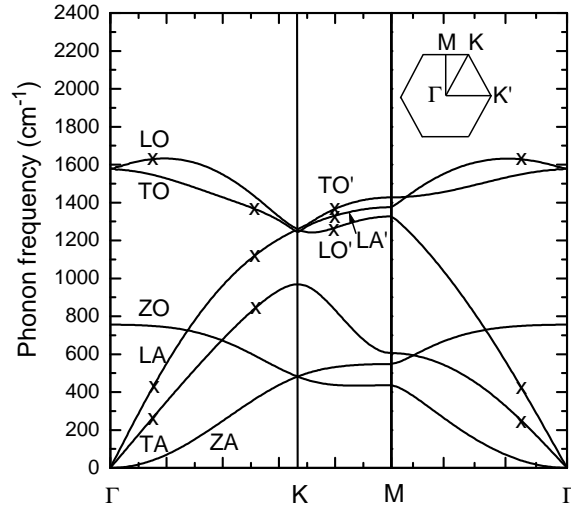


FIG. 1. Calculated phonon dispersion of graphene along the high-symmetry directions in the Brillouin zone.²² The six phonon branches are marked by the acronyms LO, TO, ZO, LA, TA, and ZA. The letters O and A stand for “optical” and “acoustic”, respectively; L, T, and Z denote in-plane longitudinal, in-plane transverse, and out-of-plane atomic displacement, respectively. The crosses mark the phonons which play major role in the DR processes. Inset: the hexagonal Brillouin zone of graphene with the special points Γ , M, K, and K' .

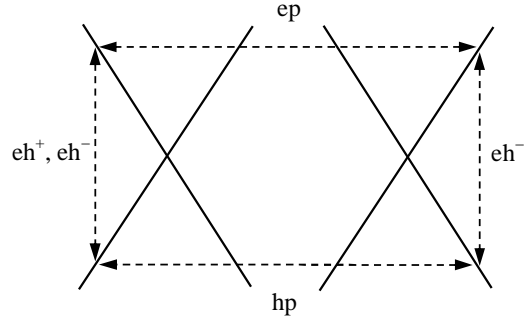


FIG. 2. Schematic representation of the DR processes in graphene. The solid lines are a cross-section of the Dirac cones at the K and K' points of the Brillouin zone. The dashed lines are virtual processes: “ eh^+ ” and “ eh^- ” are electron (e) - hole (h) creation and annihilation processes, respectively; “ ep ” and “ hp ” are electron and hole scattering processes by a phonon (p). DR processes can also take place between bands at the K or K' point only.

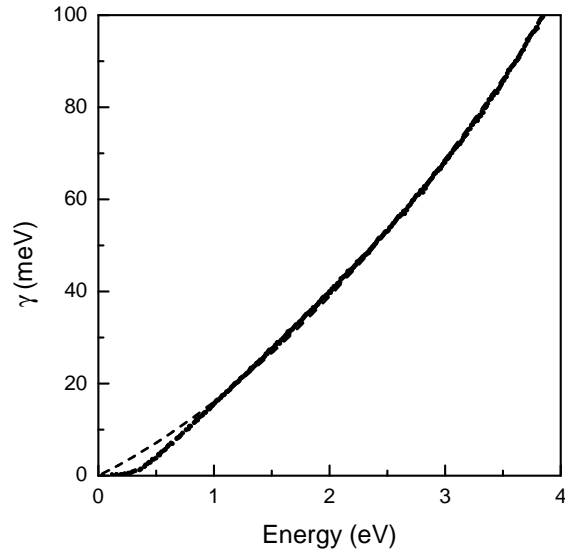


FIG. 3. Calculated electronic linewidth $\gamma(E)$ (solid symbols). The dashed line is a fit to the calculated data. The fitting function is given by Eq. (3).

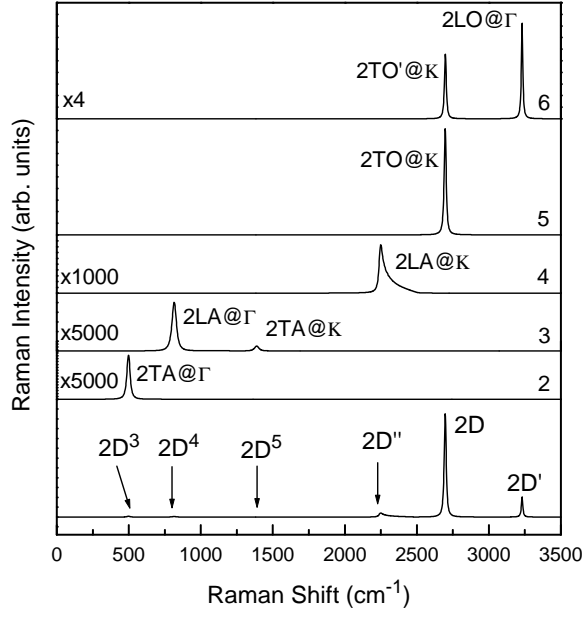


FIG. 4. Calculated overtone Raman spectrum for $E_L = 2.0$ eV (bottom). The contributions from phonons with $\nu = 2, \dots, 6$ are shown in the top graphs. The notation of the Raman bands $2D^3$, $2D^4$ and $2D^5$ is taken from Ref. [17].

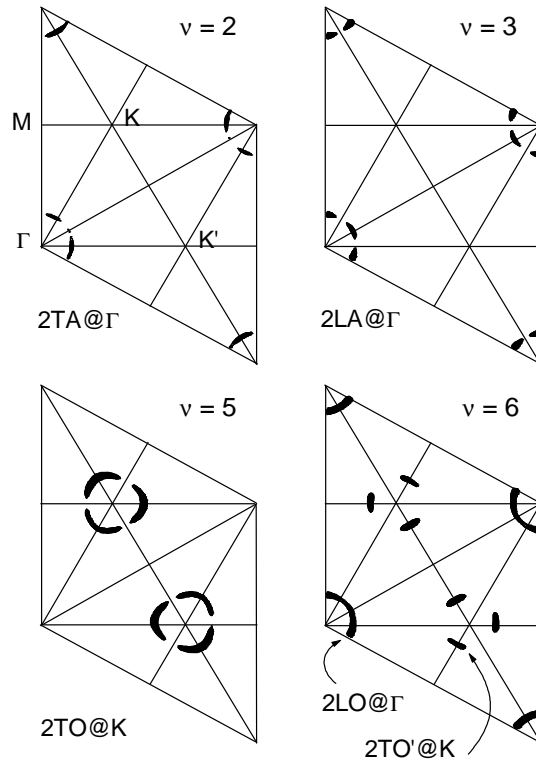


FIG. 5. The contribution to the overtone bands from phonons with $\nu = 2, 3, 5, 6$ from different parts of the rhombic Brillouin zone of graphene. The graph for $\nu = 4$ for phonons $2LA@K$ (not shown) is similar to that for $\nu = 5$.

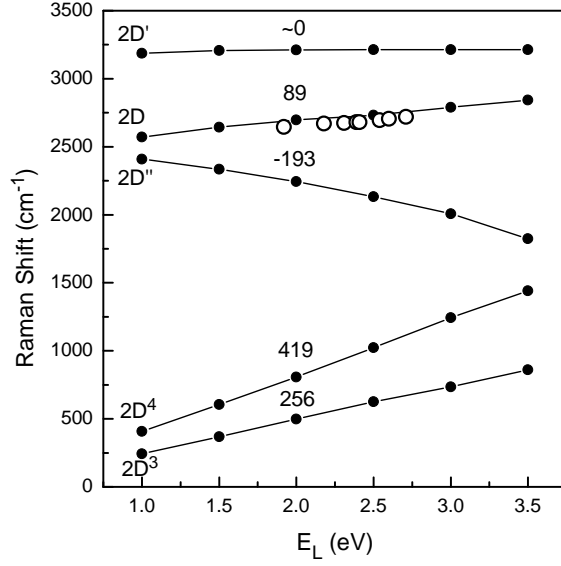


FIG. 6. Calculated dependence of the Raman shift of the overtone bands on E_L (solid symbols). The numbers are the slopes of the curves for $E_L = 2.0$ eV. The empty symbols are experimental data.¹¹

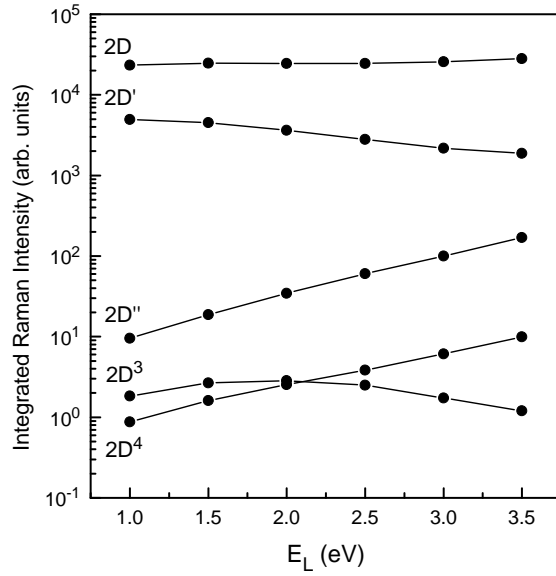


FIG. 7. Calculated dependence of the integrated Raman intensity of the overtone bands on E_L (solid symbols).

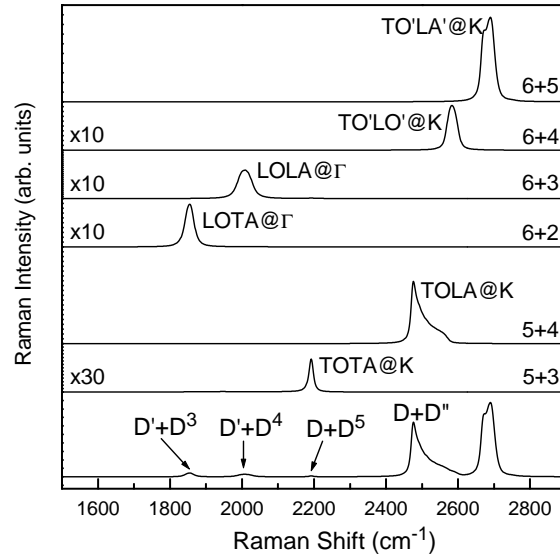


FIG. 8. Calculated combination Raman spectrum for $E_L = 2.0$ eV (bottom). The contributions from pairs of phonons with $\nu + \nu' = 5 + 3, \dots, 6 + 5$ are shown in the top graphs.

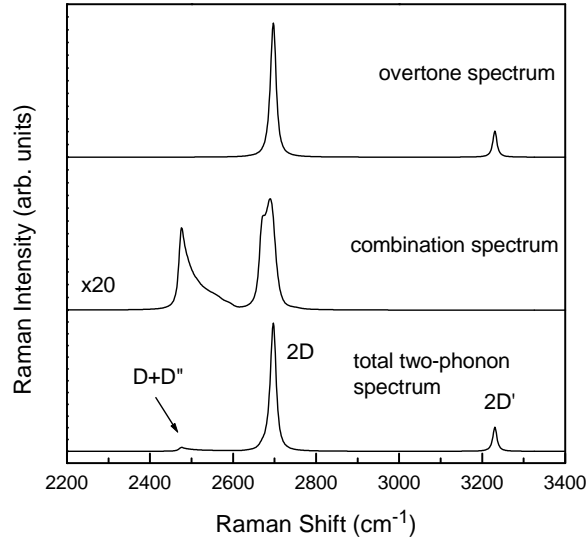


FIG. 9. Calculated total two-phonon Raman spectrum for $E_L = 2.0$ eV (bottom). The constituting combination and overtone spectra are also shown (middle and top).

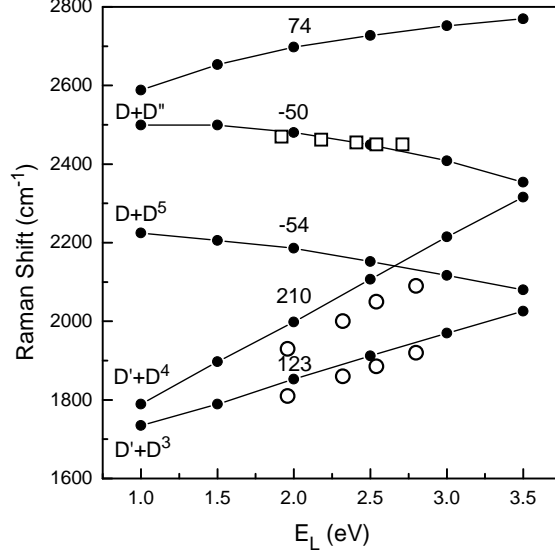


FIG. 10. Calculated dependence of the Raman shift of the combination bands on E_L (solid symbols). The highest-frequency band is due to $\text{TO}'\text{LA}'\text{@K}$ phonons. The numbers are the slopes of the curves for $E_L = 2.0$ eV. The empty symbols - squares¹¹ and circles,³⁰ are experimental data.

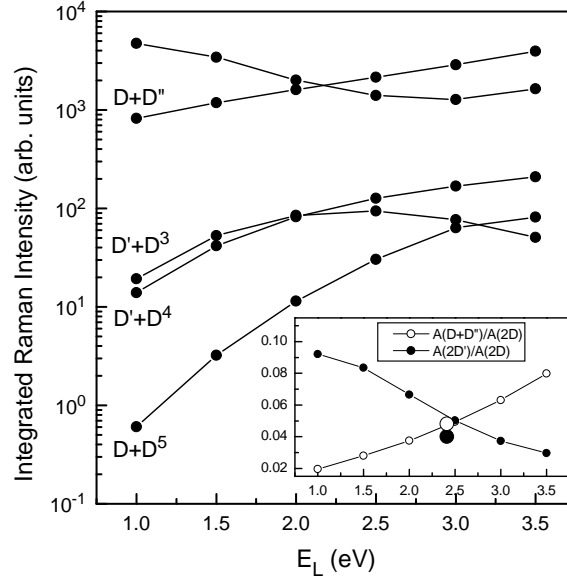


FIG. 11. Calculated dependence of the integrated Raman intensity of the combination bands on E_L (solid symbols). The highest-intensity band at low energies is due to $\text{TO}'\text{LA}'\text{@K}$ phonons. Inset: The DFT-GW corrected ratios $A(2D')/A(2D)$ and $A(D+D'')/A(2D)$ (small symbols) in comparison with experimental data³ (large symbols). The scale is the same as in Fig. 7.

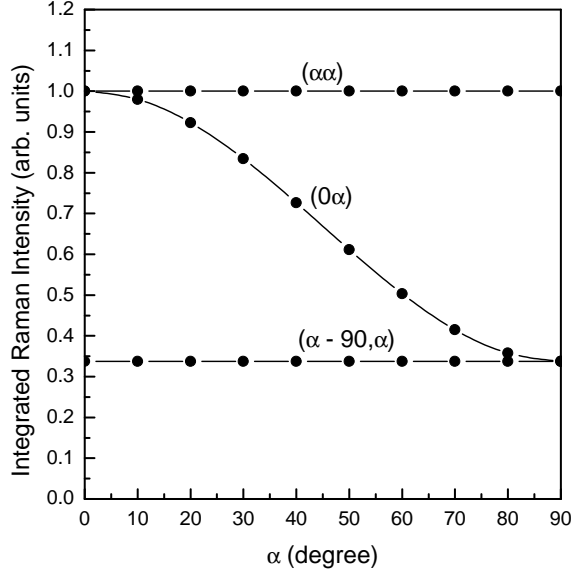


FIG. 12. Calculated polarization dependence of the integrated Raman intensity of the 2D band (solid symbols). The angle α is relative the x axis along a zigzag line of carbon bonds. The polarizer and analyzer angles are given by the notation $(\alpha\beta)$. The curves for parallel and cross polarization, $(\alpha\alpha)$ and $(\alpha - 90, \alpha)$, as well for fixed polarizer direction along the x axis and variable analyzer orientation (0α) are shown. The solid line for polarization (0α) is a fit of Eq. (4). The obtained ratio of the integrated intensities is $A_{\perp}/A_{\parallel} \approx 0.34$.